Phys. Status Solidi B **246**, No. 1, 206–214 (2009) / **DOI** 10.1002/pssb.200844013

physica status solidi b
www.pss-b.com
basic solid state physics

Synthesis of $MnGeO_3$ polycrystalline and single-crystal samples and comparative analysis of their magnetic properties

N. V. Sapronova[*,1], N. V. Volkov[,1,2], K. A. Sablina[1], G. A. Petrakovskii[1,2], O. A. Bayukov[1,2], A. M. Vorotynov[1], D. A. Velikanov[1], A. F. Bovina[1], A. D. Vasilyev[1], and G. V. Bondarenko[1]**

[1] Kirensky Institute of Physics, SB RAS, 660036 Krasnoyarsk, Russia
[2] Siberian Federal University, 660079 Krasnoyarsk, Russia

Received 9 January 2008, revised 21 July 2008, accepted 20 August 2008
Published online 9 October 2008

PACS 71.55.Ak, 75.50.Ee, 76.80.+y, 81.10.Dn

[*] Corresponding author: e-mail stasha-83@yandex.ru, Phone: +7 3912 907 108, Fax: +7 3912 438 923
[**] e-mail volk@iph.krasn.ru, Phone: +7 3912 907 525, Fax: +7 3912 438 923

$MnGeO_3$ single crystals have been grown by a flux method. The obtained $MnGeO_3$ is orthorhombic; a P_{bca} space group does not undergo any structural phase transitions in the range from room temperature to 900 °C. Magnetic measurements carried out for the first time on the $MnGeO_3$ single crystal have revealed higher values (T_N = 38 K and $\theta = -100$ K) as compared to the data for polycrystalline samples reported in the literature (T_N = 10 K and 14 K, $\theta = -54$ K and -46 K). These magnetic parameters for polycrystalline samples synthesized by us are close to the literature data. A Mössbauer spectrum taken at T = 300 K for a sample containing 5% $Fe_2^{57}O_3$ shows that manganese ions, Mn^{2+}, occupy two nonequivalent positions and iron is included in a sublattice as Fe^{2+} and distributed among two positions substituting Mn^{2+}. In this study, the magnetic characteristics are shown to be sensitive even to minor impurity amounts. The $MnGeO_3$ magnetic structure and one of possible reasons causing the effect of impurities on the $MnGeO_3$ magnetic properties are considered in the framework of a simple indirect coupling model.

1 Introduction Recent intense interest in oxide compounds containing manganese ions has been caused, first of all, by the colossal magnetoresistance phenomenon in manganese-bearing mixed-valence perovskite compounds and by the multiferroic properties discovered in $DyMnO_3$, $TbMnO_3$, etc. with Mn^{3+} [1] and in $MnWO_4$ with Mn^{2+} [2].

Among manganese oxides, there are compounds that exhibit magnetoelectricity. Magnetoelectric materials may be defined as materials that reveal a linear correlation between electric field and magnetization, as well as between magnetic field and electric polarization. In particular, the formation of magnetoelectric domains in $Mn_{0.94}Mg_{0.06}GeO_3$ single crystals has been reported [3]. Previously, the magnetoelectric effect in $MnGeO_3$ polycrystalline samples below T_N was observed [4].

This study is devoted to the investigation of the magnetic properties of $MnGeO_3$ single crystals grown by a flux method. These crystals are characterized by orthorhombic symmetry stable up to 900 °C [5]. The first measurements of the magnetic and resonance properties were carried out. They showed higher values of magnetic phase transition temperature T_N and asymptotic temperature θ for our crystals as compared to polycrystalline samples. The magnetic characteristics of the polycrystalline $MnGeO_3$ samples grown by us are the closest to those reported in [6, 7]. All the samples have the orthorhombic structure at room temperature with similar values of unit cell parameters. In contrast to the single crystals grown by us using a flux method, single crystals obtained by a floating-zone method [8] have monoclinic symmetry at room temperature. A transition from the high-temperature orthorhombic structure to the monoclinic one occurs at a temperature of about 200 °C. For this reason, the single crystals are weak and tend to break into small pieces. The authors stabilize the orthorhombic phase at room temperature by using Mg impurities.

In this study, we attempt to explain a discrepancy between the magnetic properties of single-crystal and polycrystalline samples by sensitivity to synthesis conditions.

Table 1 Technological parameters.

compound	charge composition (wt%)				temperature regime			Refs.
	MnO	GeO_2	SiO_2	$MnCl_2$	T_{max} (°C)	exposure at T_{max} (h)	cooling rate v_{cool} (°/h)	
$MnGeO_3$ (s/c)	5.3	7.7	–	87	1050	2	20	this work
$MnGeO_3$ (p/c)	41	59	–	–	1000	12	100	this work
$MnGeO_3$ (p/c)	41	59	–	–	1000	12	100	[7]
$MnGe_{0.88}Si_{0.12}O_3$ (s/c)	8	11	2	79	1050	2	20	this work

Magnetoelectric measurements on $MnGeO_3$ single crystals are planned to be carried out in the future.

2 Experimental Manganese germanate single crystals (s/c) were obtained by a flux growth method generally used for growing single crystals of high-melting oxide compounds by spontaneous crystallization.

In order to avoid redox processes in a Mn–O system with manganese valence alteration, which are inevitable upon heating in air, we developed a method of hermetization of a flux crucible using a specially designed structure from alundum crucibles whose interwall spaces are filled with kaolin wool mixed with B_2O_3 (Fig. 1).

To eliminate possible contamination of single crystals by ions of solvents (B_2O_3, PbO, BaO, PbF_2, etc. and their combinations) conventionally used in the flux growth method, we took $MnCl_2$ with the melting temperature T_{melt} = 615 °C as a solvent.

Polycrystalline (p/c) $MnGeO_3$ samples were obtained by agglomeration of MnO and GeO_2 mixed in the equimolar ratio 1:1 in an evacuated quartz vessel. Technological conditions are described in detail in Ref. [7]. The parameters of the technological regime are given in Table 1.

The $MnGeO_3$ single crystals were 0.6 × 0.2 × 0.2 cm^3 in maximum size, brown, transparent, and had the form of needles extended along the *c*-axis.

The crystal structure of the samples obtained was determined with an X-ray DRON-2 facility for powder samples and a SMART APEX (Bruker AXS) autodiffractometer for single crystals. All the X-ray patterns taken at room temperature show that all samples have a single-phase peroxene-type structure without any impurity phase. According to the results of polarization microscopy, the crystal is biaxial with the absence of twinning.

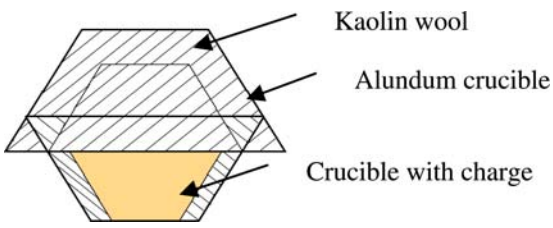

Figure 1 Crucible structure for $MnGeO_3$ single-crystal growth.

The temperature dependence of the specific magnetization was determined with a SQUID magnetometer in the temperature range 4.2–200 K in a magnetic field of 500 Oe. The measurements were performed on polycrystalline samples, individual single crystals, and powders made by grinding single crystals.

Mössbauer measurements were carried out at room temperature with a Co^{57} (Cr) source on a $MnGeO_3$ powder enriched with a Fe^{57} isotope. Mössbauer spectrum parameters were obtained by fitting a model spectrum to experimental one. The model spectrum was formed on the basis of the maximum and specific features of a distribution function of quadrupole splitting probabilities, which were determined from experimental spectra. The measured chemical shifts are given relative to αFe.

EPR spectra were taken with a Radiopan SE/X-2544 spectrometer operating in the X-range at temperatures from 78 to 300 K at different orientations of magnetic field with respect to the crystal axes.

3 Results and discussion

3.1 Crystal structure The X-ray measurements data are presented in Tables 2–4.

The symmetry transformations used for obtaining equivalent atoms are:

#1 (x, 3/2 – y, 1/2 + z); #2 (x, 1/2 – y, 1/2 – z);
#3 (1 – x, 1 – y, –z); #4 (3/2 – x, 1 – y, z – 1/2);
#5 (3/2 – x, y – 1/2, z); #6 (1 – x, 1 – y, 1 – z);
#7 (3/2 – x, 1 – y, 1/2 + z); #8 (1 – x, 1/2 + y, 1/2 – z);
#10 (x, 1/2 – y, 1/2 + z); #11 (3/2 – x, 1/2 + y, z).

In Table 4 some distances and angles decisive for the estimation of the exchange interactions in $MnGeO_3$ are given.

The $MnGeO_3$ compound also possesses the pyroxene structure typical of such well-known minerals as $MnSiO_3$, $MgSiO_3$, and others. The pyroxene structure is characterized by germanium chains of the following type: germanium atoms surrounded by four oxygen atoms form oxygen tetrahedra GeO_4, which are connected via common vertices into an infinite series. Two atoms of the oxygen tetrahedron appear common, while the two others can make bonds with manganese ions, Mn^{2+}. The manganese atoms, in their turn, are in an octahedral surrounding of oxygen atoms (MnO_6) in two nonequivalent positions. The octahedra create two-step zigzag ladders (strips) extended along the *c*-axis (Fig. 2).

Table 2 Experimental parameters and quality of the refinement of a model of the $MnGeO_3$ crystal structure.

radiation	Mo K_α (0.71073 Å)
angle range	$4.24° \le 2\theta \le 46.54°$
reflection indices interval	$-21 \le h \le 21$; $-10 \le k \le 9$; $-5 \le l \le 6$
number of reflections measured/including independent ones	3565/689 (R_{int} = 0.0359)
refinement uncertainty factors for the reflections with $I \ge 2\sigma$/for all the reflections	$R1$ = 0.0251/0.0263 wR2 = 0.0675/0.0685
Goodness of fit, GooF	1.118
extinction coefficient	0.0033(3)
maximum/minimum difference electronic density (e/Å^3)	0.663/−0.689

Table 3 Relative coordinates ($\times 10^4$) and heating parameters U_{eq} (Å$^2 \times 10^3$) of atoms of the crystal $MnGeO_3$. $U_{eq} = 1/3(U_{11} + U_{22} + U_{33})$.

atom	x/a	y/b	z/c	U_{eq}
Ge(1)	7295(1)	6570(1)	346(1)	6(1)
Ge(2)	4729(1)	3375(1)	2011(1)	6(1)
Mn(1)	6235(1)	3457(1)	−1406(2)	7(1)
Mn(2)	6223(1)	5186(1)	3511(2)	9(1)
O(1)	5631(2)	3404(4)	1951(7)	7(1)
O(2)	8193(2)	6604(4)	232(7)	7(1)
O(3)	4319(2)	4857(4)	3203(7)	9(1)
O(4)	4452(2)	1890(4)	3900(7)	8(1)
O(5)	6942(2)	7754(4)	−1857(7)	9(1)
O(6)	6904(2)	4901(4)	447(7)	11(1)

For comparison, in Table 5 the X-ray data for the $MnGeO_3$ samples synthesized by us and those reported in the literature are presented. It must be noted here that DTA (differential thermal analysis) measurements reveal no structural transitions in the range from room temperature to 1070 K [5]. It can be seen from Table 5 that the lattice constants of our $MnGeO_3$ samples are in good agreement with the literature data for $MnGeO_3$ with orthorhombic symmetry.

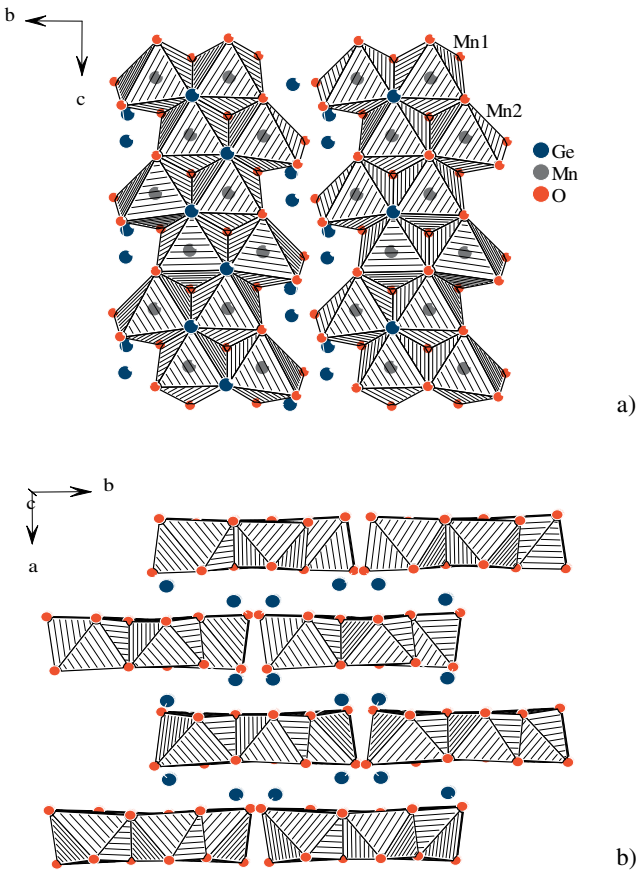

Figure 2 (online colour at: www.pss-b.com) Projections of the $MnGeO_3$ crystal structure onto: a) the *b,c*-plane, b) the *a,b*-plane. Mn ions are in octahedra.

3.2 Magnetic properties In Fig. 3 we present the temperature dependences of magnetization for the $MnGeO_3$ single crystal in three directions of magnetic field H = 500 Oe and for the $MnGeO_3$ powder.

Below $T \sim 40$ K pronounced magnetization anisotropy is observed. In the case of the magnetic field applied parallel to the two relatively perpendicular directions in the *ab-plane* (curves 2 and 3), magnetization decreases at temperature below $T \sim 40$ K. The temperature behavior of the magnetization with the magnetic field directed along the *c*-axis (curve 1) is not typical of an antiferromagnetic. Such behavior of the magnetization remains unexplained at the present time. However, we only might assume the presence of some paramagnetic Mn^{2+} ions in the samples. The synthesis conditions may apparently lead to minor displacements of manganese atoms and breaking of some Mn−O bonds. The authors of [11] explain the predisposition of the $MnGeO_3$ crystal structure to structural transitions from the rhombic phase to the monocline one and the occurrence of the intermediate forms between these structures in an isomorphic $MgSiO_3$ compound by different degrees of extension of the oxygen chains and breaking of the Mg−O bonds. Despite the above-mentioned peculiarities of the temperature dependence of the magnetization below 38 K, the anisotropic behavior of this dependence is typical for antiferromagnetics. We carried out the magnetic measurements on samples from the several synthesis series and good reproducibility of the results was obtained. Thus, we can claim that transition temperature (T = 38 K) is the Neel temperature T_N for our single crystals. One of the measured single crystals was ground into powder; then, the temperature dependence of the magnetization was taken in the same temperature range. As is seen in Fig. 3 (curve 4), the temperature of the transition to the magnetically ordered state did not change after grinding. Figure 4 shows, for example, the temperature dependence of the reciprocal susceptibility for the **2** direction from Fig. 3.

Table 4 Some interatomic distances (Å) and angular parameters (deg) in the $MnGeO_3$ structure.

atoms	distance	atoms	distance
Ge(1)–O(6)	1.713(4)	Ge(2)–O(3)	1.708(4)
Ge(1)–O(2)	1.727(4)	Ge(2)–O(1)	1.735(4)
Ge(1)–O(5)	1.760(4)	Ge(2)–O(4)	1.794(4)
Ge(1)–O(5)$^{\#1}$	1.784(4)	Ge(2)–O(4)$^{\#2}$	1.796(4)
Mn(1)–O(6)	2.109(4)	Mn(2)–O(3)$^{\#6}$	2.075(4)
Mn(1)–O(3)$^{\#3}$	2.124(4)	Mn(2)–O(6)	2.140(4)
Mn(1)–O(2)$^{\#4}$	2.140(4)	Mn(2)–O(1)	2.172(4)
Mn(1)–O(1)	2.170(4)	Mn(2)–O(2)$^{\#7}$	2.205(4)
Mn(1)–O(2)$^{\#5}$	2.219(4)	Mn(2)–O(5)$^{\#1}$	2.356(4)
Mn(1)–O(1)$^{\#2}$	2.256(4)	Mn(2)–O(4)$^{\#8}$	2.426(4)
atoms	angle	atoms	angle
Mn(1)–O(1)–Mn(2)	92.0(1)	Mn(1)$^{\#7}$–O(2)–Mn(1)$^{\#11}$	96.4(2)
Mn(1)–O(1)–Mn(1)$^{\#10}$	94.5(2)	Mn(2)$^{\#4}$–O(2)–Mn(1)$^{\#11}$	98.7(2)
Mn(2)–O(1)–Mn(1)$^{\#10}$	98.6(2)	Mn(2)$^{\#6}$–O(3)–Mn(1)$^{\#3}$	99.3(2)
Mn(1)$^{\#}$–O(2)–Mn(2)$^{\#4}$	94.9(2)	Mn(1)–O(6)–Mn(2)	94.6(2)

Table 5 Structural and magnetic properties.

compound	cell parameters, Å	space group	T_N (K)	θ (K)	μ_{eff}, μ_B	Refs.
$MnGeO_3$, s/c	a = 19.25, b = 9.23, c = 5.46	Pbca	38	$\theta_{\parallel} = -97$; $\theta_{\perp 2} = -110$; $\theta_{\perp 3} = -100$	6.0	this work
powder obtained by grinding of a s/c $MnGeO_3$	a = 19.130, b = 9.273, c = 5.415	Pbca	38	−110	5.77	this work
$MnGeO_3$ p/c obtained using the technology from Ref. [13]	a = 19.223, b = 9.286, c = 5.426	Pbca	18	−46	5.57	this work
$MnGeO_3$, p/c	a = 19.245, b = 9.228, c = 5.437	Pbca	16	−46	5.48	[6]
$MnGeO_3$, p/c	a = 19.23, b = 9.24, c = 5.45	Pbca	10	−54	6.0	[7]
$MnGeO_3$ p/c	a = 19.267, b = 9.248, c = 5.477	Pbca	–	–	–	[9]
$MnGeO_3$ s/c-bundles	a = 19.29, b = 9.25, c = 5.48	Pbca	–	–	–	[10]
$MnGe_{0.88}Si_{0.12}O_3$, s/c	a = 19.296, b = 9.278, c = 5.476	Pbca	18	−50	6.21	this work

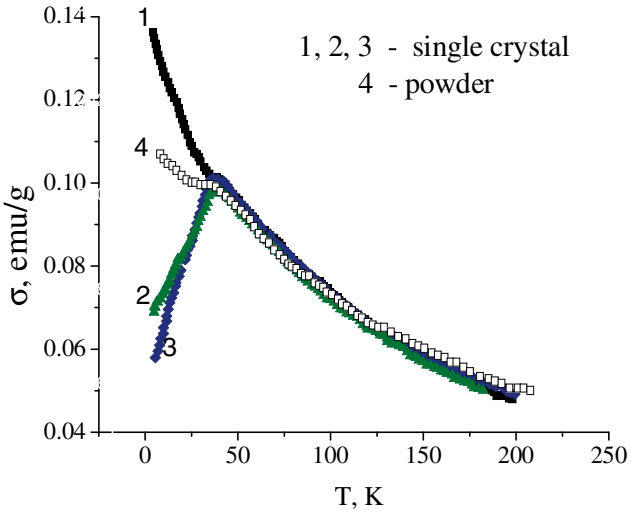

Figure 3 (online colour at: www.pss-b.com) Temperature dependence of the magnetization in the field of 500 Oe for the $MnGeO_3$ single crystal and the powder obtained by grinding of the single crystal.

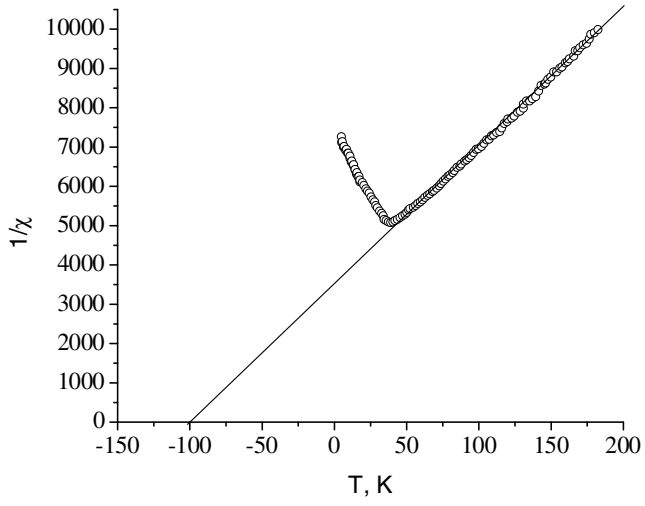

Figure 4 Temperature dependence of reciprocal susceptibility for the **2** direction of $MnGeO_3$ [7].

In the temperature range 125–200 K the reverse susceptibility curve is characterized by a linear dependence and obeys the Curie–Weiss law $\chi = C/(T-\theta)$. Using this relation, $\mu_{eff} = 6.0\mu_B$ were calculated, which is typical for Mn^{2+}(S = 5/2). The asymptotic Curie temperatures θ = –100 K were determined by extrapolation of a linear part of the reciprocal susceptibility to the cross point with a temperature axis. In Table 5 are listed θ values for all directions. As is seen from Table 5 the θ values for the single-crystal sample and the powder obtained by grinding of the single-crystal $MnGeO_3$ were found to be twice the literature data for some polycrystalline samples [6, 7]. T_N behaves appropriately, which evidences strengthening of the exchange interaction in our samples.

To clarify the origin of such a giant discrepancy between the magnetic properties of our samples and those of the polycrystalline samples described in the literature, we synthesized a polycrystalline $MnGeO_3$ sample using the technology reported in [7]. The temperature dependence of the magnetization for this sample is given in Fig. 5. It is seen that the temperature of magnetization maximum (T_N = 20 K) is substantially lower than that for the single crystal but higher than those reported in [6] (T_N = 16 K) and [7] (T_N = 10 K).

Such a discrepancy in the magnetic characteristics may be caused by the different synthesis conditions. First, it is noteworthy that all the polycrystalline samples were synthesized in quartz vessels. We suppose that the polycrystalline $MnGeO_3$ samples are contaminated with silicon ions. As is well known, SiO_2 is soluble in GeO_2 over a wide concentration range [12]. Upon complete substitution of germanium by silicon the well-known $MnSiO_3$ compound with T_N = 7 K is obtained [7]. In order to verify the effect of silicon on the $MnGeO_3$ magnetic properties, $MnGeO_3$ single crystals with silicon impurity introduced into the solution-melt as SiO_2 were grown. The presence of silicon in our polycrystalline samples was confirmed by X-ray fluorescent analysis. The chemical formula and lattice constants of these single crystals were determined by an X-ray study (see Table 5). The temperature dependences for the $MnGe_{0.88}Si_{0.12}O_3$ single crystal are shown in Fig. 6. The just-noticeable kink of the curves in the vicinity of $T \sim 40$ K may be caused by the presence of even minor amounts of the ferrimagnetic phase Mn_3O_4 with T_N = 40 K.

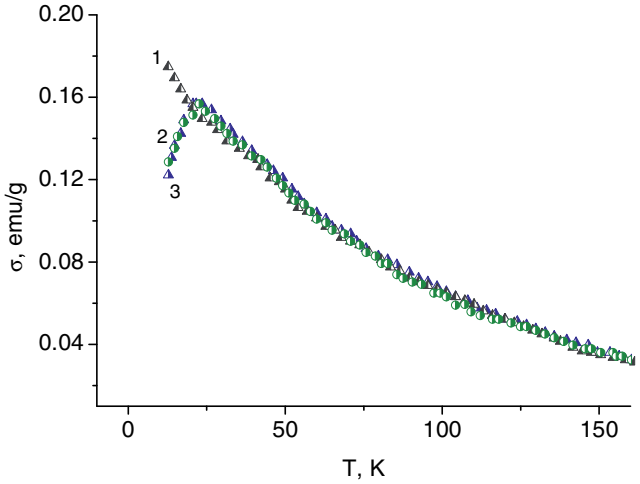

Figure 6 (online colour at: www.pss-b.com) Temperature dependence of magnetization H = 500 Oe for the $MnGe_{0.88}Si_{0.12}O_3$ single crystal: curve 1 – $H \parallel c$, curves 2, 3 – magnetic field applied parallel to the two relatively perpendicular directions in the a,b-plane.

Thus, the availability of silicon in $MnGeO_3$ reduces T_N. Therefore, we may assume that the $MnGeO_3$ magnetic properties are sensitive even to minor amounts of impurity, at least in a germanium subsystem.

3.3 Mössbauer measurements Mössbauer measurements were carried out on $Mn_{0.99}Fe^{57}{}_{0.01}GeO_3$ samples. The Mössbauer spectrum (Fig. 7) measured on a powder

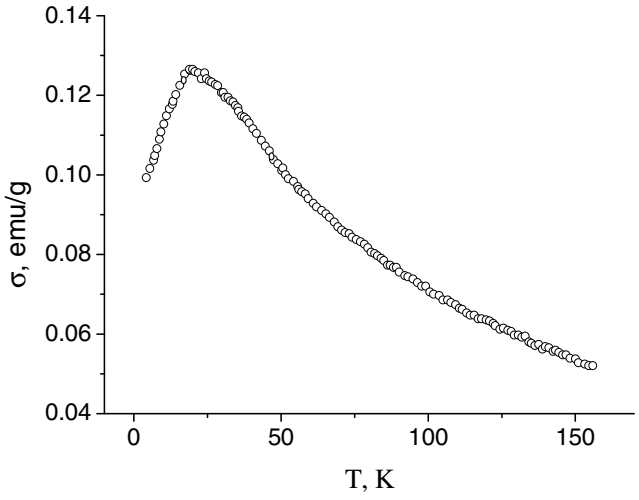

Figure 5 Temperature dependence of magnetization in H = 500 Oe for the polycrystalline $MnGeO_3$ sample.

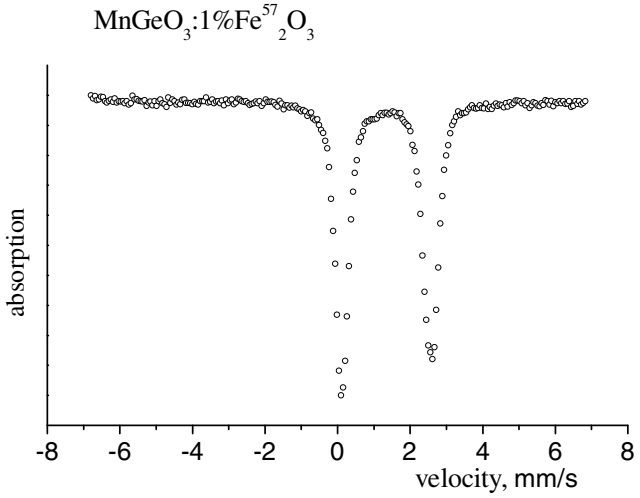

Figure 7 $MnGeO_3$ Mössbauer spectrum taken at room temperature.

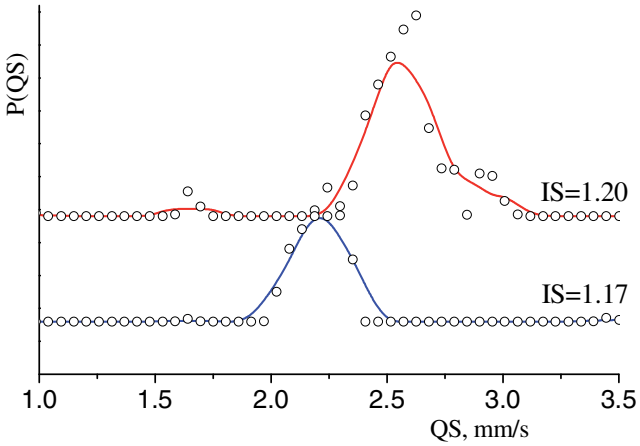

Figure 8 (online colour at: www.pss-b.com) Distribution of the quadrupole splitting probability in the $MnGeO_3$ Mössbauer spectrum.

absorber represents an asymmetric quadrupole doublet. Since the doublet linewidths are different, one might assume that the doublet asymmetry is caused by the presence of nonequivalent iron positions in the crystal rather than by the Goldanskii–Karyagin effect.

Refinement of a spectrum is made by a fitting of a model spectrum to an experimental one using the least-squares method. For construction of the model spectrum the probability of quadrupole splittings P(QS) is restored from the experimental spectrum. To find the distribution P(QS) the sum of two groups of doublets with various chemical shifts is used. On obtaining P(QS) from experimental data both the amplitudes and the chemical shifts that are similar for two groups of doublets were fitted (Fig. 8). These results allowed us to define the values of chemical shifts and quadrupole splittings. On the second step of refinement the model spectrum was fitted to the experimental one at a variation of all sets of hyperfine parameters. The results of refinement are given in Table 6. As is seen from Table 6 in this crystal we have two nonequivalent positions of iron differing in degrees of both a covalent bond and distortion of the local surrounding, which is in good agreement with the data presented in [6].

Here, IS is the isomer chemical shift with respect to αFe, QS is the quadrupole splitting, W is the absorption linewidth at half-height, and S is the fractional occupancy of a position by iron. Mn1 and Mn2 mean the crystallographic positions in $MnGeO_3$.

The magnitude of the isomer chemical shift for two different positions of the crystal confirms that the impurity iron enters into $MnGeO_3$ as Fe^{2+}. Both positions are octahedral but have different degrees of distortion and electronic densities at a site. Comparative analysis of the Mössbauer and X-ray structural data makes it possible to easily identify these positions. As the X-ray data show, the oxygen octahedron is distorted more strongly around the Mn2 position than around Mn1 one. Correspondingly, quadrupole splitting that characterizes a distortion degree of local surrounding for the Fe2 position is noticeably larger than that for the Fe1 position. Moreover, the X-ray data evidence that the mean distances in the coordination octahedra are Mn1–O = 2.17 Å and Mn2–O = 2.23 Å. A smaller interionic distance implies that the bond between Mn1 and a lattice is more covalent as compared to that between M2 and a lattice. This result correlates with the Mössbauer data. A smaller magnitude of the chemical shift for the Fe1 position means that at this site the electronic density on an iron nucleus is higher and, consequently, the bond covalence degree is also higher. It is interesting to note that if in pure $MnGeO_3$ populations of Mn1 and Mn2 positions are equal so the Fe^{2+} preference to the distorted Mn2 position is twice that to the symmetric Mn1 position. Probably, this is related to asymmetry of a $3d^6$ electron shell of the Fe^{2+}, in contrast to a symmetric $3d^5$ shell of the Mn^{2+}.

3.4 EPR spectra The spectrum consists of a single Lorenz line with the following parameters at room temperature: $\Delta H_\perp$ = 345 Oe, $\Delta H_\parallel$ = 375 Oe, $g_\perp$ = 2.00, and $g_\parallel$ = 2.01 ($\parallel$ and $\perp$ denote the orientation of the external magnetic field parallel to the crystal c-axis and an arbitrary orientation of the external magnetic field perpendicular to the c-axis, respectively). The angular dependence of the magnetic resonance linewidth at room temperature is shown in Fig. 9a. It has a period $\pi/2$ in the plane where the c-axis lies and is well described by the function $\Delta H \sim A\,(1 + \cos^2\theta)$ typical for magnetoconcentrated compounds with an orthorhombic unit cell. The angular dependence of a resonance field is illustrated in Fig. 9b.

The temperature dependences of the linewidth and resonance field for different orientations of the external magnetic field in the temperature range 80–300 K are presented in Fig. 10. A broadening of the magnetic resonance linewidths is observed, which is caused by growth of fluctuations of local fields on manganese ions. Apparently, the magnetic field resonance linewidth increases up to the temperature of the magnetic phase transition and then broadens crucially in accordance with the theoretical models [13, 14].

Table 6 Hyperfine parameters of the $MnGeO_3$:Fe^{57} Mössbauer spectra.

position	IS ± 0.02 mm/s	QS ± 0.04 mm/s	W ± 0.02 mm/s	S ± 0.05
Fe1(Mn1)	1.17	2.23	0.33	0.37
Fe2(Mn2)	1.20	2.58	0.35	0.63

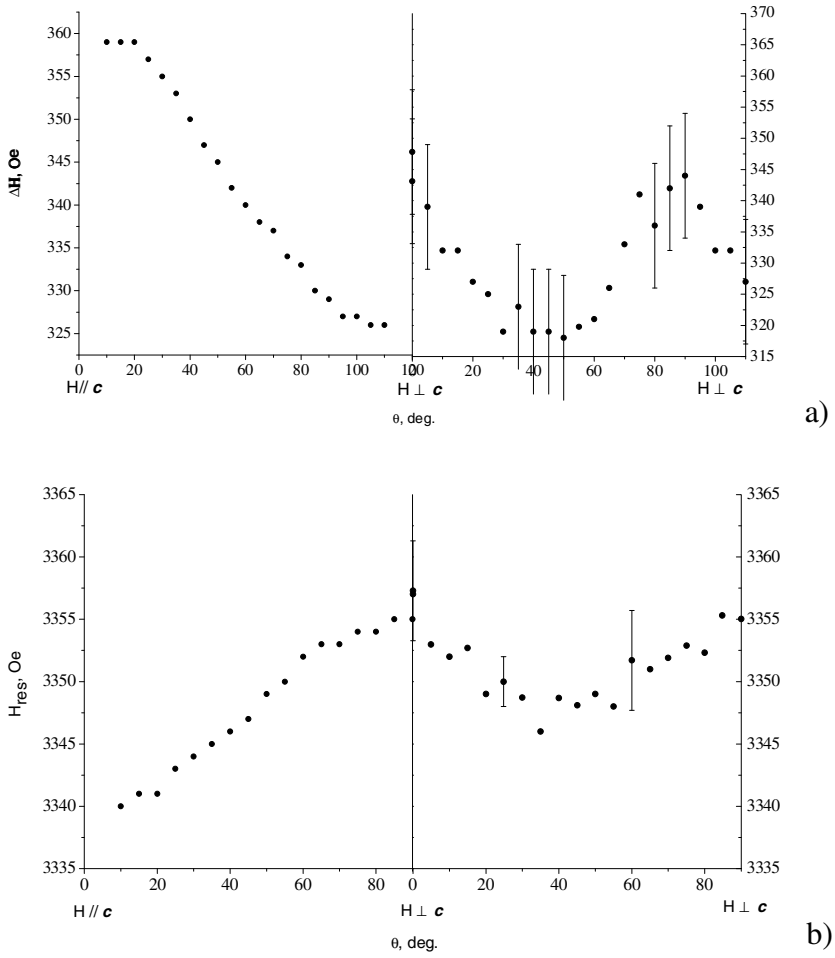

Figure 9 Angular dependences of a) the $MnGeO_3$ single crystal linewidth, b) resonance field of the $MnGeO_3$ single crystal at room temperature.

With decreasing temperature the resonance field value increases when the magnetic field is oriented perpendicular to the crystal *c*-axis and decreases in the case of the parallel orientation. Calculations of the second moment M_2 of the absorption line for manganese ions in the $MnGeO_3$ lattice within the point dipole model with regard to a number of the nearest neighbors in both the ladder and neighboring ladders yield the values $M_2 \sim 3.62 \times 10^{+7} - 1.8 \times 10^{+7}$ Oe^2 for different directions of the magnetic moments relative to the crystal axes. The linewidth value at room temperature is estimated as $\Delta H \sim \sqrt{M_2} \sim 6000-4250$ Oe. Disagreement of these values with the experimental data evidences substantial exchange narrowing of the magnetic resonance linewidth, so that $\Delta H \sim \sqrt{M_2}/J$, where J is the magnitude of the effective exchange field on manganese ions. The estimation of a J magnitude gives the values $J \sim 12-17$ K.

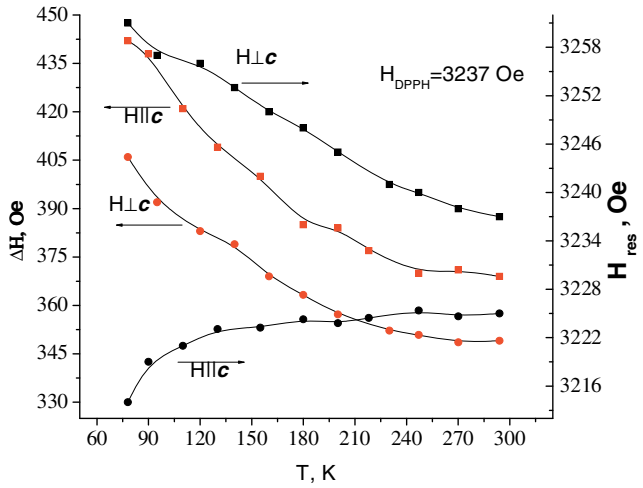

Figure 10 (online colour at: www.pss-b.com) Temperature dependences of the linewidth ΔH and resonance field H_{res} of the $MnGeO_3$ single crystal.

3.5 $MnGeO_3$ magnetic structure The exchange interactions in $MnGeO_3$ can be described in the framework of the indirect coupling model by two exchange integrals [15]: (i) the exchange integral for short pathway (Mn–O–Mn) J, and (ii) the exchange integral for long pathway (Mn–O–Ge–O–Mn) G. The J integral describes the 90° exchange interactions between Mn cations within the ladder. In the case of a d^5 electronic configuration of cations this integral is negative (the interaction is antiferromagnetic):

$$J = -\tfrac{2}{75}\, c(8b + 3c)\, U_{Mn} |\cos \varphi| \,, \qquad (1)$$

where b, c are parameters of the ligand–cation electron transfer for σ- and π-bonds, respectively; each of them represents a squared coefficient of admixing of the ligand atomic wavefunction to the cation wavefunction. U_{Mn} is the energy of oxygen–manganese electron excitation; φ is the Mn–O–Mn bond angle. In the structure of $MnGeO_3$ the Mn–O distances are different, they range between 2.109 Å and 2.257 Å. The Mn–O–Mn bond angles also vary between 91.96° and 98.74°. To simplify analysis we neglected these distinctions in the lengths and angles, and we considered only a number of indirect couplings. Magnetic coupling between the ladders in a crystal is realized through multiple Mn–O–Ge–O–Mn superexchange pathways, and it can be described by the G exchange integral. This integral is also negative when cations have d^5 configuration:

$$G = -\tfrac{4}{25}\, g^2 \left(\tfrac{8}{9}\, b^2 + c^2\right) (U_{Ge} + U_{Mn})\, |\cos\varphi_1|\, |\cos\varphi_2|\,, \quad (2)$$

where g is the parameter of oxygen–germanium electron transfer, U_{Ge} is the energy of the oxygen–germanium electron excitation, φ_1 and φ_2 are the Mn–O–Ge bond angles in the multiple pathways. Here, we again neglected distinctions in bond distances and bond angles, and considered only the number of indirect couplings. Since b, c and $g \ll 1$ the G integral is much smaller than J and, consequently, the interladder interactions are much weaker than intraladder exchange interactions. Both the intraladder and interladder indirect exchange couplings within the bc-plane are presented schematically in Fig. 11. The number of lines designates the number of bonds (pathways).

At first, let us consider the intra-ladder couplings described by the J integral. We can see that Mn1 has five neighbors connected antiferromagnetically, and Mn2 has only three neighbors connected antiferromagnetically. In that case, the interactions, which define the relative orientation of the cation moments within ladders, are the Mn1–Mn1 interactions via "diagonal" bonds and the Mn1–Mn2 interactions via bonds along "guiding line", along the c-axis, of the ladder (Fig. 11). The interactions along the b-axis of the ladder (Mn1–Mn2) are found frustrating. Thus, we can conclude that only six exchange couplings for Mn1 described by J and two ones for Mn2 mainly determine the magnetic structure of the crystal.

Now, let us consider the interladder exchange interactions within the b,c-plane described by the integral G (Fig. 11). We can see that Mn2 cations in neighboring ladders are coupled via "diagonal" bonds ($3G$). These Mn2–Mn2 interactions determine completely the relative orientation of the magnetic moments of the ladders. The interactions Mn1–Mn2 ($2G$) are found frustrating. Thus, only four exchange couplings described by G determine the ordering of the moments of the ladders within the b,c-plane.

Finally, let us consider interladder interactions described by G integrals for a ladder located in neighboring planes along the a-axis. The Mn1 cation in each plane is coupled via eleven bonds with manganese cations situated in nearest planes, upper and lower, through intermediate Ge1 and Ge2 layers, respectively (Fig. 2a). Here, Mn1 has six bonds with Mn↑ cations and by five bonds with Mn↓ cations. Thus, only one bond contributes mainly to the magnetic ordering. The Mn2 cation in each plane has thirteen bonds with the manganese cations situated in the nearest planes through the intermediate Ge1 layers, seven bonds with Mn↑ and six bonds with Mn↓ cations. Thus, only one of the thirteen bond contributes to ordering. The Mn2 cation also has eight bonds with Mn↑ and five bonds with Mn↓ through the Ge3 layer, and, consequently, three bonds contribute to the arrangement of magnetic moments in the structure of the crystal.

A lot of the frustrating exchange couplings, probably, defines the low temperature limit of magnetic ordering in $MnGeO_3$. The $MnGeO_3$ magnetic structure predicted by the simplified indirect coupling model is shown in Fig. 12. It is

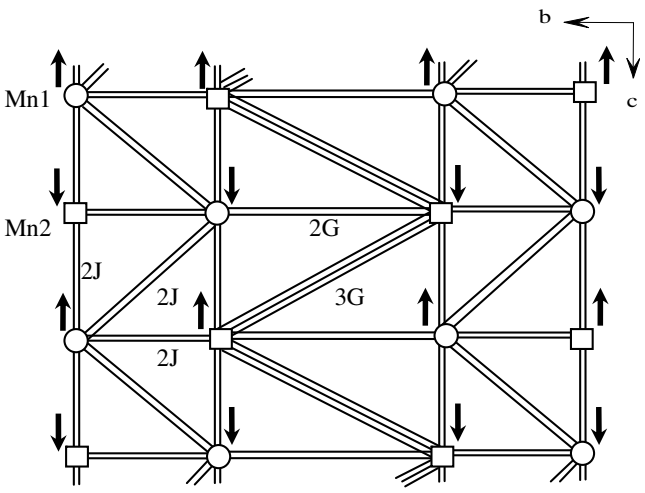

Figure 11 Schematic view of the indirect exchange couplings between the nearest neighbors in the $MnGeO_3$ structure.

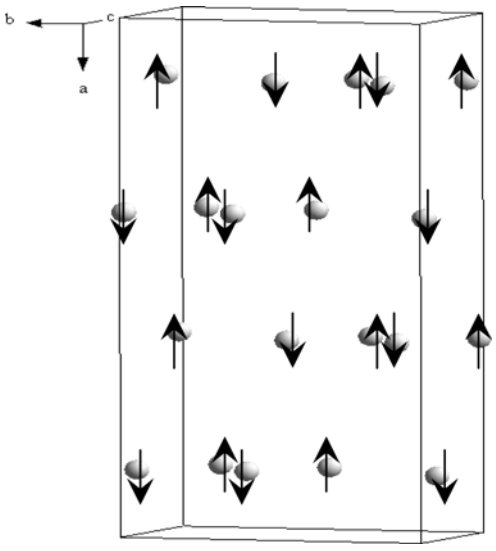

Figure 12 Magnetic structure of $MnGeO_3$.

compatible with the magnetic structure refined from neutron diffraction data [6].

Upon substitution of Ge by Si the average distances in an oxygen octahedron increase from 2.17 Å up to 2.189 Å for Mn–O and from 2.23 Å up to 2.245 Å for Mn2–O. This extension of the exchange couplings is the most probable reason for a T_N decrease.

On the basis of data on a destroying silicon effect on the spin-Peierls temperature in $CuGeO_3$, the authors of [16] claim that the substitution of germanium by silicon can break the superexchange interactions between the neighboring copper chains in the places of Si location or change this interaction from antiferromagentic to ferromagnetic. It can be imaged also that the difference between the Si and Ge ionic radii results in lattice distortion in a radius of several lattice constants and, thus, may strongly modify the magnetic properties.

4 Conclusion Data of the magnetic measurements on single-crystal and polycrystalline $MnGeO_3$ samples presented in this paper have demonstrated, first of all, the importance of obtaining pure single crystals for samples certification. For the first time, the $MnGeO_3$ single crystals grown by a flux method with the use of $MnCl_2$ as a solvent have revealed a considerable difference between the exchange interaction magnitudes and magnetic phase transition temperatures as compared to the literature data for polycrystalline $MnGeO_3$. Now we can claim with a high degree of confidence that $MnGeO_3$ is the antiferromagnetic with $T_N = 38$ K, $\theta \sim -100$ K, and $\mu_{eff} = 6.0\mu_B$.

Acknowledgements This study was supported by the Integration project CO No 3.7. The authors also thank the Russian Foundation for Science Support.

References

[1] T. Goto, T. Kimura, G. Lawes, A. P. Ramirez, and Y. Tokura, Phys. Rev. Lett. **92**, 257201 (2004).
[2] O. Heyer, N. Hollmann, I. Klassen, S. Jodlauk, L. Bohaty, P. Becker, J. A. Mydosh, T. Lorenz, and D. Khomskii, J. Phys.: Condens. Matter **18**, L471 (2006).
[3] P. J. Brown, J. B. Forsyth, and F. Tasset, Solid State Sci. **7**, 682 (2005).
[4] G. Gorodetsky, Phys. Lett. A **39**, 155 (1972).
[5] A. M. Vorotynov, G. A. Petrakovskii, K. A. Sablina, D. A. Velikanov, L. V. Udod, A. D. Vasiliev, A. F Bovina, and N. V. Sapronova, EASTMAG-2004. Abstract book, 194 (2004).
[6] P. Herpin and A. Whuler, phys. stat. sol. (b) **44**, 71 (1971).
[7] A. Sawaoka, S. Miyahaka, and S. Akimoto, J. Phys. Soc. Jpn. **25**, 1253 (1968).
[8] H. Matsumura, M. Mamiya, and H. Takei, J. Cryst. Growth **210**, 783 (2000).
[9] J. H. Fang and W. D. Townes, Z. Kristallogr. **130**, 139 (1969).
[10] A. Tauber, J. A. Kohn, C. G. Whinfrey, and W. D. Babbage, Am. Mineral. **48**, 555 (1963).
[11] U. Bregg and G. Klaringbull, Crystal Structure of Minerals (Mir, Moscow, 1967).
[12] N. A. Toropov, P. B. Barzakovskii, V. V. Lapin, and N. N. Kurtseva, State Diagrams of the Silicate Systems (Nauka, Moscow, Leningrad, 1965).
[13] G. F. Kokoszka, Low-dimensional Cooperative Phenomena (Plenum Press, New York and London, 1976).
[14] P. M. Richards and M. B. Salamon, Phys. Rev. B **9**, 32 (1974).
[15] O. A. Bayukov and A. F. Savitskii, phys. stat. sol. (b) **155**, 249 (1989).
[16] D. Khomskii, W. Geertsma, and M. Mostovoy, Czech. J. Phys. **46**, Suppl. S6, 3240 (1996).

